Contribution from the Department of Chemistry, Memorial University of Newfoundland, St. John's, Newfoundland, Canada A1B 3X7, and the National Research Council, Ottawa, Ontario, Canada K1A 0R6

Copper Coordination Chemistry of Novel Octadentate, Tetranucleating, Bis(diazine) Ligands. Structural and Magnetic Properties of Tetranuclear Complexes Involving a Rectangular Array of Copper(II) Centers

Santokh S. Tandon,[1a] Sanat K. Mandal,[1a] Laurence K. Thompson,*[,1a] and Rosemary C. Hynes[1b]

Received July 30, 1991

The potentially octadentate, tetranucleating ligands 1,4,6,9-tetrakis((R-2-pyridyl)amino)benzodipyridazine (TNLR: TNL (R = H), TNL4 (R = 4 Me), TNL5 (R = 5Me), TNL4E (R = 4Et)) bond four copper(II) centers in a rectangular structure involving two distant copper pairs in one molecular entity in the derivatives $[Cu_4(L)(\mu_2\text{-}OH)_2(H_2O)_8](CF_3SO_3)_6$ (L = TNL4 (I), TNL5 (IV)), $[Cu_4(TNL)(\mu_2\text{-}OH)_2(H_2O)_6(EtOH)_2](CF_3SO_3)_6$ (II), $[Cu_4(TNL)(\mu_2\text{-}OH)_2(NO_3)_4](NO_3)_2\cdot 2H_2O$ (III), $[Cu_4(TNL4)(\mu_2\text{-}OH)_2(H_2O)_2Br_6]$ (V), and $[Cu_4(TNL4E)(\mu_2\text{-}Cl)_4Cl_4]$ (VI). Variable-temperature magnetic studies indicate strong local, intrapair antiferromagnetic coupling in the hydroxide-bridged compounds but also the presence of significant, distant, interpair antiferromagnetic coupling across the benzodipyridazine ring system. Exchange in the chloro-bridged complex (VI) is dominated by weak ferromagnetic coupling. The crystal and molecular structures are reported for $[Cu_4(TNL4)(\mu_2\text{-}OH)_2(H_2O)_8](CF_3SO_3)_6\cdot 6H_2O$ (I) and $[Cu_4(TNL)(\mu_2\text{-}OH)_2(H_2O)_6(EtOH)_2](CF_3SO_3)_6$ (II). I crystallizes in the monoclinic system, space group $I2/m$, with a = 10.813 (9) Å, b = 26.204 (15) Å, c = 13.489 (15) Å, β = 98.73 (8)°, and two formula units per unit cell. II crystallizes in the monoclinic system, space group $I2/m$, with a = 11.907 (3) Å, b = 19.858 (3) Å, c = 15.965 (4) Å, β = 105.31 (2)°, and two formula units per unit cell. In both structures pairs of square-pyramidal copper centers are bridged by a hydroxide and diazine unit with Cu-OH-Cu angles of 116.3° (I) and 116.0° (II) and Cu-Cu separations of 3.202 Å (I) and 3.190 (2) Å (II).

Introduction

Complexes in which a single ligand can organize several metals into a polynuclear cluster are of particular interest, especially if the metals can undergo at least a one-electron redox step at thermodynamically accessible potentials. The arrangement of the metals, dictated by the ligand, could enable small molecular substrates to be affected by several metals at once, with the possibility of multiple electron transfer to and from the substrate. Catalytic processes under such conditions could, with appropriate molecular design, have high efficiency.

Binucleating ligands are common, trinucleating ligands are less common, but tetranucleating ligands are rare. A tetranucleating macrocyclic ligand derived by template (Ba^{2+}) condensation of 2,6-diacetylpyridine with 1,3-diamino-2-hydroxypropane, followed by transmetalation with $Mn(ClO_4)_2\cdot 6H_2O$, has been shown to give a tetranuclear complex with a $Mn_4(alkoxy)_4$ core.[2] A related tetranuclear macrocyclic copper(II) complex has also been synthesized by template condensation of 2,6-diformyl-4-*tert*-butylphenol and 1,5-diamino-3-hydroxypentane in the presence of $Cu(NO_3)_2\cdot 3H_2O$. In this complex the planar arrangement of four coppers is bridged peripherally by two phenoxo and two alkoxo oxygens and internally by a μ_4-hydroxo group.[3] A related perchlorate complex involving the same ligand was shown to contain two similar macrocyclic units with a central μ_4-oxo group[4] coupled together as a dimeric entity to give what is essentially an octanuclear complex. Tetranuclear nickel and zinc complexes of a related macrocyclic ligand have been prepared by the template condensation of 2,6-diformyl-4-methylphenol and 2,6-bis(aminomethyl)-4-methylphenol in the presence of the appropriate metal acetate in methanol. Each complex had a central μ_4-hydroxo bridge.[5]

Our experience with binuclear copper complexes revealed that ligands based on substituted phthalazines and pyridazines produced binuclear centers, which underwent spontaneous two-electron reductions at positive potentials (vs SCE) and displayed, in some cases, close to electrochemical reversibility.[6-9] The additional observation that, in some cases, catalytic behavior was demonstrated for the air oxidation of catechols[7] encouraged us to pursue the synthesis of related ligands that were capable of binding more than two metals in similar environments.

In this report we describe the synthesis of members of a new class of tetranucleating, tetrapyridyl benzodipyridazine ligands (Figure 1) (1,4,6,9-tetrakis((R-2-pyridyl)amino)benzodipyridazine (TNLR: TNL (R = H), TNL4 (R = 4Me), TNL5 (R = 5Me), TNL4E (R = 4Et))), which is an extension of a previous method used to synthesis related 1,4-bis(pyridylamino)phthalazines.[10-13] A route to the tetrapyridyl benzodipyrrole precursors has already been reported.[14] Reaction of the ligands with excess copper salts in water, alcohol, or mixed alcohol/water solvents produced tetranuclear copper(II) complexes involving hydroxide and halogen bridges. A preliminary report of the structure and some properties of $[Cu_4(TNL4)(\mu_2\text{-}OH)_2(H_2O)_8](CF_3SO_3)_6\cdot 6H_2O$ has already been published.[15]

Experimental Section

Synthesis of Ligands and Complexes. (a) 1,3,5,7-Tetrakis((4-ethyl-2-pyridyl)imino)benzodipyrrole (Figure 1A, R = 4-Ethyl-2-pyridyl). Tetracyanobenzene[16] and 2-amino-4-ethylpyridine were reacted together according to the literature procedure,[14] which involved reaction in methanol and then butanol in the presence of anhydrous calcium chloride over a period of 16 days. However, a rather low yield of the product was obtained by this long, laborious route and so the following, quicker, procedure was adopted.

* To whom correspondence should be addressed.

(1) (a) Memorial University of Newfoundland. (b) National Research Council.
(2) McKee, V.; Shepard, W. B. *J. Chem. Soc., Chem. Commun.* **1985**, 158.
(3) McKee, V.; Tandon, S. S. *J. Chem. Soc., Chem. Commun.* **1988**, 385.
(4) McKee, V.; Tandon, S. S. *Inorg. Chem.* **1989**, *28*, 2901.
(5) Bell, M.; Edwards, A. J.; Hoskins, B. F.; Kachab, E. H.; Robson, R. *J. Am. Chem. Soc.* **1989**, *111*, 3603.
(6) Thompson, L. K.; Mandal, S. K.; Rosenberg, L.; Lee, F. L.; Gabe, E. J. *Inorg. Chim. Acta* **1987**, *133*, 81.
(7) Thompson, L. K.; Mandal, S. K.; Gabe, E. J.; Lee, F. L.; Addison, A. W. *Inorg. Chem.* **1987**, *26*, 657.
(8) Woon, T. C.; McDonald, R.; Mandal, S. K.; Thompson, L. K.; Connors, S. P.; Addison, A. W. *J. Chem. Soc., Dalton Trans.* **1986**, 2381.
(9) Mandal, S. K.; Woon, T. C.; Thompson, L. K.; Newlands, M. J.; Gabe, E. J. *Aust. J. Chem.* **1986**, *39*, 1007.
(10) Thompson, L. K.; Chacko, V. T.; Elvidge, J. A.; Lever, A. B. P.; Parish, R. V. *Can. J. Chem.* **1969**, *22*, 4141.
(11) Bautista, D. V.; Dewan, J. C.; Thompson, L. K. *Can. J. Chem.* **1982**, *60*, 2583.
(12) Bullock, G.; Hartstock, F. W.; Thompson, L. K. *Can. J. Chem.* **1983**, *61*, 57.
(13) Bautista, D. V.; Bullock, G.; Hartstock, F. W.; Thompson, L. K. *J. Heterocycl. Chem.* **1983**, *20*, 345.
(14) Gagné, R. R.; Marritt, W. A.; Marks, D. N.; Siegl, W. O. *Inorg. Chem.* **1981**, *20*, 3260.
(15) Tandon, S. S.; Mandal, S. K.; Thompson, L. K. *J. Chem. Soc., Chem. Commun.* **1991**, 1572.
(16) Epstein, A.; Wildi, B. S. *J. Chem. Phys.* **1960**, *32*, 324.
(17) Germain, G.; Main, P.; Woolfson, M. M. *Acta Crystallogr., Sect. A: Cryst. Phys., Diffr., Theor. Gen. Crystallogr.* **1971**, *A27*, 368.

0020-1669/92/1331-2215$03.00/0

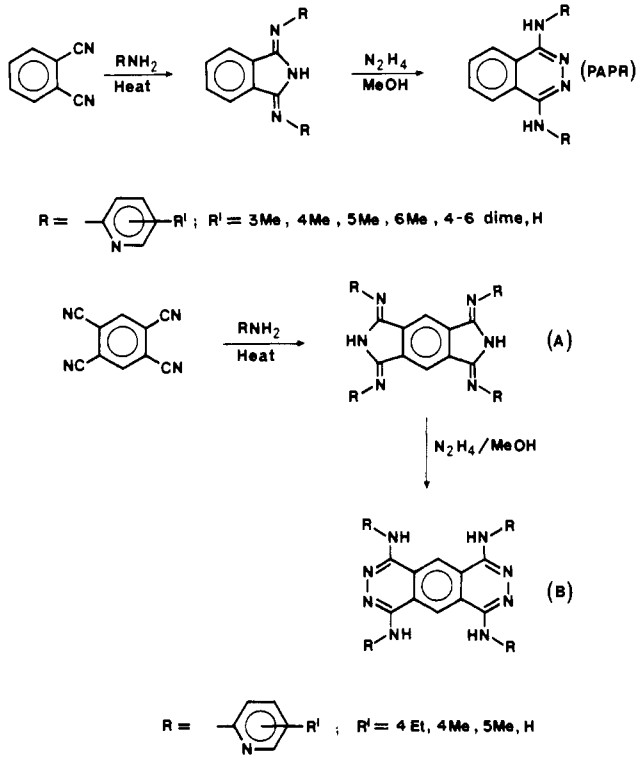

Figure 1. Synthetic routes to pyridyl phthalazines and pyridyl benzodipyridazines.

Tetracyanobenzene (1.8 g, 1.0×10^{-2} mol) and 2-amino-4-ethylpyridine (9.8 g, 8.0×10^{-2} mol) were heated together, in the presence of a catalytic amount of P_2S_5, at 120 °C for 3 days. The dark, solid product was crushed, washed with diethyl ether and acetone to remove unreacted starting materials, and extracted with $CHCl_3$. Reduction in volume of this solution produced the intermediate benzodipyrrole (yield 1.6 g, 25%). Anal. Calcd for $C_{38}H_{36}N_{10}\cdot 3.5H_2O$: C, 65.59; H, 6.23; N, 20.13. Found: C, 65.65; H, 5.99; N, 20.05.

(b) 1,4,6,9-Tetrakis((4-ethyl-2-pyridyl)amino)benzodipyridazine (Figure 1B, R = 4-Ethyl-2-pyridyl (TNL4E)). 1,3,5,7-Tetrakis((4-ethyl-2-pyridyl)imino)benzodipyrrole (1.6 g) was heated with excess 85% hydrazine hydrate (5 mL) in methanol (10 mL) at reflux for 3 days. The resulting mixture was cooled and filtered and the residual solid washed with methanol and extracted into hot chloroform. The volume of the resulting yellow solution was reduced to ~100 mL and petroleum ether (40–60) added to induce crystallization of a yellow solid (mp 275–280 °C; yield 1.0 g, 60%). Anal. Calcd for $C_{38}H_{38}N_{12}\cdot 3.5H_2O$: C, 62.88; H, 6.25; N, 23.16. Found: C, 62.90; H, 5.75; N, 23.49. Major fragments were found in the mass spectrum, corresponding to the molecular ion and reasonable degradation fragments, at the following masses: 662 (P), 646, 541, 419, 391, 331, 314, 299, 271, 181, 122, 106, 80. NMR (302 K, CD_2Cl_2/TMS), chemical shift (ppm) (relative intensity): 1.25 (24) (triplet, CH_3), 2.60 (16) (quartet, CH_2), 6.67 (8) (doublet, pyridine H5), 8.03 (8) (doublet, pyridine H_6). Two broad resonances are observed at 7.47 (~13) and 9.0 (~7) ppm, with a weak, sharp singlet superimposed on the higher field resonance at 7.33 ppm. The total intensity of these peaks corresponds to the remaining pyridine (H_3), NH, and benzene ring protons.

The other ligands were prepared by a similar route, but because of their limited solubility, purification was effected by Soxhlet extraction into chloroform to give yellow or orange solids. Yields of the benzodipyrroles exceed 90%, while yields of the benzodipyridazines are ~75%. Melting points exceed 320 °C (not recorded) for TNL4 and TNL5, with a darkening in color to dark brown above 300 °C. TNL changes in color from orange to brown above 220 °C and melts with decomposition in the range 290–310 °C. Molecular ion peaks and peaks associated with reasonable fragments were observed in the mass spectra of TNL, TNL4, and TNL5. Anal. Calcd for $C_{30}H_{22}N_{12}\cdot 2.5H_2O$ (TNL): C, 60.50; H, 4.54; N, 28.24. Found: C, 60.37; H, 4.19; N, 28.61.

(c) $[Cu_4(TNL4)(\mu_2\text{-}OH)_2(H_2O)_8](CF_3SO_3)_6$ (I). TNL4 (0.20 g, 0.33 mmol) was added to a solution of $Cu(CF_3SO_3)_2$ (1.0 g, 2.8 mmol) in water (100 mL) and the mixture stirred at room temperature for 15 h. The green solution was filtered to remove unreacted ligand and concentrated to ~5 mL under reduced pressure. Green crystals formed on standing overnight, which were filtered, washed with a small amount of water, and dried under vacuum. Anal. Calcd for $C_{40}H_{42}N_{12}O_{25}F_{18}S_6Cu_4$: C, 25.56; H, 2.23; N, 8.94. Found: C, 25.50; H, 2.34; N, 9.00. This analysis corresponds to the formula $[Cu_4(TNL4)(\mu_2\text{-}OH)_2(H_2O)_5](CF_3SO_3)_6$, which was used in the magnetic calculations. The crystals crumble readily on drying, losing lattice solvent, and the X-ray sample was kept in contact with mother liquor prior to crystallographic analysis. Compounds II–IV were prepared similarly. A mixture of solvents (H_2O/EtOH) was used for II. Anal. Calcd for $C_{40}H_{54}N_{12}O_{31}F_{18}S_6Cu_4$ (II): C, 24.17; H, 2.73; N, 8.46; Cu, 12.79. Found: C, 23.85; H, 2.44; N, 8.58; Cu, 12.94. Anal. Calcd for $C_{30}H_{28}N_{18}O_{22}Cu_4$ (III): C, 28.89; H, 2.25; N, 20.22; Cu, 20.34. Found: C, 29.04; H, 2.41; N, 20.13; Cu, 19.82. Anal. Calcd for $C_{40}H_{48}N_{12}O_{28}F_{18}S_6Cu_4$ (IV): C, 24.84; H, 2.48; N, 8.70; Cu, 13.15. Found: C, 24.59; H, 2.53; N, 8.51; Cu, 14.01.

(d) $[Cu_4(TNL4)(\mu_2\text{-}OH)_2Br_6(H_2O)_2]$ (V). Solid TNL4 (0.20 g, 0.33 mmol) was added to a solution of $CuBr_2$ (1.0 g, 4.4 mmol) in water (100 mL) and the mixture refluxed for 24 h. A green, microcrystalline solid formed, which was filtered, washed with water, and dried under vacuum. Anal. Calcd for $C_{34}H_{36}N_{12}O_4Br_6Cu_4$ (V): C, 28.94; H, 2.55; N, 11.91; Cu, 18.01. Found: C, 29.26; H, 2.38; N, 11.92; Cu, 17.77.

(e) $[Cu_4(TNL4E)(\mu_2\text{-}Cl)_4Cl_4]\cdot 0.5MeOH\cdot 3H_2O$ (VI). TNL4E (0.11 g, 1.7×10^{-4} mol) was dissolved in hot methanol (600 mL) and a solution of $CuCl_2\cdot 2H_2O$ (0.17 g, 1.0×10^{-3} mol) in hot methanol (200 mL) added. When the mixture was heated on a steam bath for 4 h a green microcrystalline precipitate formed, which was filtered, washed with methanol, and dried under vacuum. Anal. Calcd for $C_{38.5}H_{46}N_{12}O_{3.5}Cl_8Cu_4$: C, 36.40; H, 3.65; N, 13.23; Cl, 22.32. Found: C, 36.45; H, 3.30; N, 13.18; Cl, 22.49.

Physical Measurements. NMR spectra were recorded with a Bruker WP80 spectrometer ($SiMe_4$ internal standard), mass spectra were obtained with a VG Micromass 7070 HS spectrometer with a direct insertion probe and electronic spectra with a Cary 17 spectrometer, C, H, N, and halogen analyses were carried out by Canadian Microanalytical Service.

Variable-temperature magnetic susceptibility data were obtained in the range 5–305 K using an Oxford Instruments superconducting Faraday magnetic susceptibility system with a Sartorius 4432 microbalance. A main solenoid field of 1.5 T and a gradient field of 10 T m^{-1} were employed. Calibration data were obtained using $HgCo(NCS)_4$.

Crystallographic Data Collection and Refinement of the Structures. (a) $[Cu_4(TNL4)(\mu_2\text{-}OH)_2(H_2O)_8](CF_3SO)_6\cdot 6H_2O$ (I). Crystals of I are green. The diffraction intensities of an approximately $0.20 \times 0.20 \times 0.15$ mm crystal, mounted in a sealed capillary, were collected with graphite-monochromatized Cu Kα radiation by using the θ/2θ scan mode to $2\theta_{max} = 119.8°$ on a Picker diffractometer. Of a total of 5236 measured reflections, 2884 were unique and 2428 were considered significant with $I_{net} > 2.5\sigma(I_{net})$. Data were corrected for decay, Lorentz, and polarization effects, but no correction was made for absorption. The cell parameters were obtained by the least-squares refinement of the setting angles of 24 reflections with $2\theta = 100–120°$ (λ (Cu Kα) = 1.540 56 Å).

The structure was solved by direct methods using SOLVER and refined by full-matrix least-squares calculations. Hydrogen atoms were located in a difference Fourier map but were not refined. All non-hydrogen atoms were refined anisotropically. In the final cycles weights based on counting statistics were used and the refinement converged with residuals $R = 0.053$ and $R_w = 0.071$. Crystal data are given in Table I, and final atomic positional parameters and equivalent isotropic temperature factors are given in Table II. All calculations were performed with the NRCVAX system of programs.[18] Scattering factors were taken from ref 19. Anisotropic thermal parameters (Table SI) and a listing of structure factors are included as supplementary material.

(b) $[Cu_4(TNL)(\mu_2\text{-}OH)_2(H_2O)_6(EtOH)_2](CF_3SO_3)_6$ (II). Crystals of II are green. The diffraction intensities of an approximately $0.30 \times 0.20 \times 0.15$ mm crystal were collected with graphite-monochromatized Mo Kα radiation by using the θ/2θ scan mode to $2\theta_{max} = 45.0°$ on an Enraf Nonius diffractometer. Data collection and refinement were carried out in a manner similar to that for I. Hydrogen atoms on the ligand and coordinated water and ethanol molecules were placed in calculated positions. The disorder in the axial ligands was modeled by assuming they are half water and half ethanol. All non-hydrogen atoms, except those in the ethanol molecules, were refined anisotropically, but all atoms were included in the refinement. Crystal data are given in Table I, and final atomic positional parameters and equivalent isotropic temperature factors are given in Table III. Anisotropic thermal parameters (Table SII) and a listing of structure factors are included as supplementary material.

(18) Gabe, E. J.; Lee, F. L.; LePage Y. In *Crystallographic Computing III*; Sheldrick, G., Kruger, C., Goddard, R., Eds.; Clarendon: Oxford, England, 1985; p 167.

(19) *International Tables for X-ray Crystallography*; Kynoch: Birmingham, England, 1974; Vol. IV, p 99, Table 2.2B.

Table I. Crystal Data

empirical formula	$Cu_4C_{40}H_{60}N_{12}O_{34}F_{18}S_6$	$Cu_4C_{40}H_{48}N_{12}O_{28}F_{18}S_6$
fw	2041.47	1933.38
cryst syst	monoclinic	monoclinic
space group	*I*2/*m*	*I*2/*m*
a, Å	10.813 (9)	11.907 (3)
b, Å	26.204 (15)	19.858 (3)
c, Å	13.489 (15)	15.965 (4)
β, deg	98.73 (8)	105.31 (2)
V, Å^3	3778 (6)	3640.8 (14)
Z	2	2
ρ(calcd), g cm^{-3}	1.795	1.764
μ, mm^{-1}	4.01	1.45
radian wavelength, Å	1.540 56	0.709 30
data collcn temp, °C	22	22
index ranges		
h	−12 to +12	−12 to +12
k	0–29	0–21
l	0–15	0–17
no. of obsd reflcns	5236	4129
no. of unique reflcns	2884	2463
no. of reflcns with $I > 2.5\sigma(I)$	2428	1780
R^a	0.053	0.066
$R_w{}^b$	0.071	0.092
goodness of fit	4.61	3.01

$^a R = \sum(|F_o| - |F_c|)/\sum(|F_o|)$. $^b R_w = [\sum w(|F_o| - |F_c|)^2/\sum w(|F_o|)^2]^{1/2}$.

Results and Discussion

Polynuclear coordination complexes often result from the serendipitous organization of a molecular mixture in which simple ligand entities, which normally behave in a monodentate fashion, utilize extra lone pairs of electrons and function in a polydentate bridging capacity. Ligands like chloride, bromide, hydroxide, azide, and thiocyanate are particularly adept in this regard. The selective use of ligand donor groups strategically placed in an organic entity can, by virtue of their juxtaposition, specifically attract more than one metal center forming a polynuclear complex. The metals can be organized into proximal groups or be separated by quite large distances. Many organic heterocycles function in this way, and the diazines pyridazine and phthalazine and their derivatives form a group that produces binuclear centers with relatively short (3.0–3.5 Å) metal–metal separations.

The design and synthesis of ligands capable of attracting two metals is relatively straightforward, but increasing that number beyond two is much more of a challenge. 1,2-Dicyanobenzene has been shown to condense smoothly with various 2-aminopyridines to produce the corresponding disubstituted 1,3-diiminoisoindolines. Ring expansion of these intermediates with hydrazine produces the corresponding phthalazines, which have been shown to behave very effectively as binucleating ligands[10–13] (Figure 1). An extension of the design of this type of ligand to produce a potentially tetranucleating system involves the use of 1,2,4,5-tetracyanobenzene, which has been shown to condense successfully with substituted 2-aminopyridines to produce the corresponding double isoindolines (benzodipyrroles), but only by template condensation methods.[14] Ligands of this type produce binuclear derivatives with manganese, iron, cobalt, nickel, and copper.[14] We have shown that ring expansion of these double isoindoline intermediates (Figure 1) can be effected by reaction with hydrazine to produce the corresponding double phthalazines (benzodipyridazines). The ligand TNL4E, which has the highest solubility in the group, has been fully characterized (see Experimental Section). This class of ligand can be considered as the superposition of two pyridylamino phthalazine ligands (Figure 1) and each phthalazine-like half can accommodate two metal centers, thus leading to a tetranuclear complex.

In order to identify the NH proton resonances in the NMR spectrum of TNL4E, a D_2O exchange experiment was carried out. Addition of D_2O to the CD_2Cl_2 solution of TNL4E caused almost complete elimination of the 9.0 ppm resonance and reduced the intensity of the peak at 7.47 ppm (see Experimental Section). The sharp singlet at 7.33 ppm showed up much more clearly and is assigned to the fused benzene ring proton. The pyridine H_3 proton is assumed to be part of the resonance at 7.47 ppm. The fact that NH resonances appear to occur at both 7.47 and 9.00 ppm indicates two types of NH proton in the ligand. A number of different tautomeric forms can be proposed for the ligand, and in fact, it may exist as a mixture of tautomers. Clearly the tautomeric mixture involves NH protons at both ring and exocyclic sites, a feature observed for the related ligand 1,4-bis(2′-pyridylamino)phthalazine and its alkylated derivatives.[13] In these compounds, NH resonances were observed at 8.7–8.8 and 6.3–7.0 ppm and were accompanied also by asymmetric benzene ring proton resonances.

Table II. Final Atomic Positional Parameters and Equivalent Isotropic Debye–Waller Temperature Factors (esd's) for $[Cu_4(TNL4)(\mu_2\text{-}OH)_2(H_2O)_8](CF_3SO_3)_6\cdot 6H_2O$ (I)

	x	*y*	*z*	$B_{iso}{}^a$
Cu	0.76693 (9)	0.56110 (3)	0.11538 (7)	3.85 (5)
S1	0.5339 (3)	1/2	−0.19092 (20)	2.97 (12)
S2	0.82366 (21)	0.67124 (8)	−0.36366 (17)	4.02 (10)
F1	0.4037 (4)	0.54040 (19)	−0.3500 (3)	6.3 (3)
F2	0.5661 (6)	1/2	−0.3792 (4)	4.8 (4)
F3	0.7650 (7)	0.5776 (3)	−0.3652 (7)	12.9 (6)
F4	0.6624 (7)	0.6199 (4)	−0.4811 (5)	15.6 (6)
F5	0.6179 (6)	0.6258 (3)	−0.3382 (5)	10.3 (4)
O1	0.8027 (6)	1/2	0.0513 (4)	3.0 (3)
O2	0.7012 (5)	0.59453 (17)	−0.0117 (3)	4.3 (3)
O3	0.9795 (5)	0.59452 (19)	0.1079 (4)	4.6 (3)
O4	0.6072 (6)	0.54452 (23)	−0.1785 (4)	7.5 (3)
O5	0.4290 (7)	1/2	−0.1432 (5)	5.3 (4)
O6	0.8704 (6)	0.66327 (25)	−0.2606 (4)	7.4 (4)
O7	0.9107 (5)	0.65978 (19)	−0.4290 (4)	4.4 (3)
O8	0.7545 (7)	0.71525 (23)	−0.3865 (6)	10.2 (5)
N1	0.7112 (5)	0.61916 (19)	0.1927 (4)	2.5 (3)
N2	0.8341 (4)	0.52628 (16)	0.2472 (3)	2.00 (22)
N3	0.8756 (5)	0.60402 (19)	0.3248 (4)	2.55 (25)
C1	0.6081 (7)	0.6459 (3)	0.1565 (5)	3.5 (3)
C2	0.5716 (7)	0.6886 (3)	0.2032 (6)	4.2 (4)
C3	0.6409 (7)	0.7048 (3)	0.2929 (6)	3.8 (4)
C4	0.7453 (7)	0.6771 (3)	0.3296 (5)	3.3 (4)
C5	0.7754 (6)	0.63354 (24)	0.2799 (5)	2.5 (3)
C6	0.5966 (9)	0.7486 (3)	0.3480 (6)	6.2 (5)
C7	0.8833 (6)	0.55203 (22)	0.3251 (4)	1.9 (3)
C8	0.9465 (5)	0.52660 (21)	0.4148 (4)	2.0 (3)
C9	1	0.5530 (3)	1/2	2.2 (4)
C10	0.4757 (12)	1/2	−0.3275 (8)	4.1 (6)
C11	0.7033 (12)	0.6229 (5)	−0.3894 (10)	7.1 (7)
OW1	0.1071 (7)	1/2	0.1477 (6)	6.1 (5)
OW2	0.7803 (7)	0.68058 (20)	−0.0810 (4)	7.8 (4)
HN3	0.935	0.621	0.365	3.2
HO1	0.831	1/2	−0.011	3.2
HO2A	0.734	0.627	−0.031	3.2
HO2B	0.667	0.578	−0.063	3.2
HO3A	1.023	0.619	0.148	3.2
HO3B	1.022	0.581	0.056	5.3
H1	0.552	0.634	0.086	4.5
H2	0.486	0.709	0.172	5.2
H4	0.805	0.689	0.398	4.3
H6A	0.557	0.773	0.309	3.2
H6B	0.660	0.768	0.371	3.2
H6C	0.566	0.739	0.409	3.2
H9	1	0.590	1/2	3.2
HOW1A	0.083	1/2	0.210	3.2
HOW1B	0.195	1/2	0.178	3.2
HOW2A	0.738	0.707	−0.093	3.2
HOW2B	0.788	0.672	−0.147	3.2

$^a B_{iso}$ is the mean of the principal axes of the thermal ellipsoid.

Description of the Structures of $[Cu_4(TNL4)(\mu_2\text{-}OH)_2(H_2O)_8](CF_3SO_3)_6\cdot 6H_2O$ (I) and $[Cu_4(TNL)(\mu_2\text{-}OH)_2(H_2O)_6(EtOH)_2](CF_3SO_3)_6$ (II). The structure of I is shown in Figure 2. Interatomic distances and angles relevant to the copper coordination spheres are given in Table IV. The structure represents a unique arrangement in which four square-pyramidal copper(II)

Table III. Final Atomic Positional Parameters and Equivalent Isotropic Debye–Waller Temperature Factors (esd's) for $[Cu_4(TNL)(\mu_2\text{-}OH)_2(H_2O)_6(EtOH)_2](CF_3SO_3)_6$ (II)

	x	y	z	B_{eq}[a]
Cu	0.41981 (12)	0.08030 (5)	0.15264 (6)	3.64 (7)
S1	0.7126 (4)	0	0.13860 (22)	4.45 (22)
S2	0.2537 (3)	0.29118 (15)	0.06598 (17)	4.92 (15)
F1	0.7551 (12)	0.0493 (6)	0.2926 (5)	15.7 (8)
F2	0.8972 (13)	0	0.2694 (10)	17.7 (18)
F3	0.2720 (8)	0.4193 (4)	0.0952 (6)	8.8 (5)
F4	0.4246 (9)	0.3747 (5)	0.0752 (7)	11.0 (7)
F5	0.2740 (9)	0.3908 (4)	−0.0326 (6)	10.4 (6)
O1	0.3445 (9)	0	0.1067 (5)	4.5 (5)
O2	0.3753 (7)	0.1221 (3)	0.0368 (4)	4.7 (4)
O3	0.2549 (8)	0.1304 (4)	0.1893 (5)	6.5 (5)
O4	0.5922 (13)	0	0.1326 (7)	9.6 (10)
O5	0.7535 (12)	0.0572 97)	0.1085 (7)	14.0 (8)
O6	0.1314 (7)	0.3002 (4)	0.0363 (5)	5.3 (4)
O7	0.2939 (8)	0.2781 (4)	0.1572 (5)	7.2 (5)
O8	0.3037 (8)	0.2491 (4)	0.0134 (5)	6.7 (5)
N1	0.5127 (7)	0.1594 (4)	0.2022 (4)	3.3 (4)
N2	0.4645 (7)	0.0346 (3)	0.2690 (4)	3.2 (4)
N3	0.4821 (7)	0.1368 (3)	0.3408 (4)	3.5 (4)
C1	0.5585 (9)	0.2002 (5)	0.1539 (6)	4.1 (5)
C2	0.6036 (10)	0.2622 (5)	0.1797 (6)	4.6 (5)
C3	0.6037 (10)	0.2831 (5)	0.2627 (7)	5.0 (6)
C4	0.5645 (10)	0.2411 (5)	0.3156 (6)	4.3 (5)
C5	0.5195 (9)	0.1795 (4)	0.2845 (5)	3.4 (5)
C6	0.4788 (8)	0.0691 (4)	0.3410 (5)	2.9 (4)
C7	0.4890 (7)	0.0346 (4)	0.4233 (5)	2.5 (4)
C8	1/2	0.0694 (5)	0.5000	2.8 (6)
C9	0.796 (3)	0	0.2541 (10)	7.4 (15)
C10	0.3115 (15)	0.3731 (7)	0.0513 (10)	7.0 (8)
CC1	0.141 (4)	0.1092 (19)	0.175 (3)	10.2 (9)
CC2	0.072 (3)	0.1082 (19)	0.099 (3)	10.6 (10)

[a] B_{eq} is the mean of the principal axes of the thermal ellipsoid.

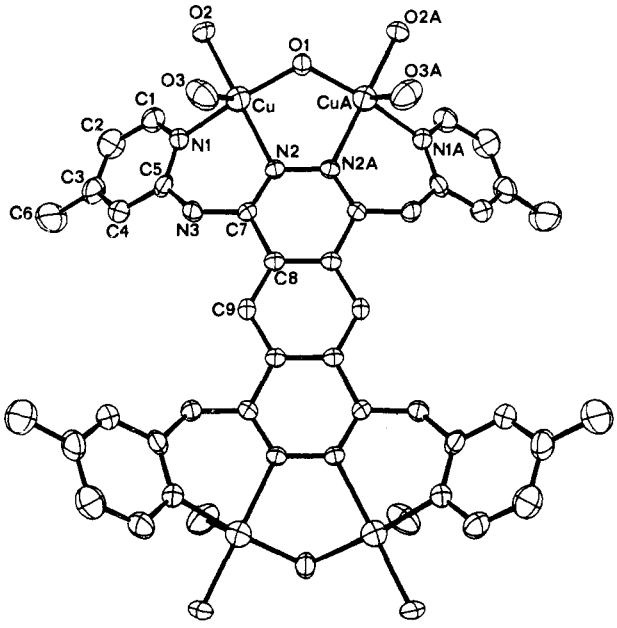

Figure 2. Structural representation of $[Cu_4(TNL4)(\mu_2\text{-}OH)_2(H_2O)_8]^{6+}$ (cation of I) with hydrogen atoms omitted (40% probability thermal ellipsoids).

ions are grouped in two pairs on opposite sides of the benzodipyridazine fragment, and within each binuclear unit the coppers are bridged equatorially by the diazine N_2 group and by a hydroxide. Two water molecules complete the copper coordination sphere with a N_2O_2 in-plane donor set. In-plane copper–ligand distances are typical for copper centers in this sort of environment, with a fairly short distance to the hydroxide bridge (1.885 (3) Å). The longer axial water contact (2.473 (5) Å) is typical for square-pyramidal copper(II) and is accompanied by a slight axial displacement of the copper from the O1–O2–N1–N2 least-squares

Table IV. Interatomic Distances (Å) and Angles (deg) Relevant to the Copper Coordination Spheres in $[Cu_4(TNL4)(\mu_2\text{-}OH)_2(H_2O)_8](CF_3SO_3)_6\cdot 6H_2O$ (I)

Cu–O1	1.885 (3)	Cu–N1	1.986 (5)	O(1)–CuA	1.885 (3)
Cu–O2	1.962 (4)	Cu–N2	2.030 (4)	Cu–CuA	3.202 (2)
Cu–O3	2.473 (5)				
O1–Cu–O2	93.14 (21)		O3–Cu–N2	89.00 (18)	
O1–Cu–O3	91.35 (21)		N1–Cu–N2	89.01 (18)	
O1–Cu–N1	171.33 (21)		Cu–O1–CuA	116.3 (3)	
O1–Cu–N2	86.85 (20)		Cu–N1–C1	121.1 (4)	
O2–Cu–O3	91.36 (19)		Cu–N1–C5	121.6 (4)	
O2–Cu–N1	90.96 (19)		Cu–N2–N2A	116.7 (3)	
O2–Cu–N2	179.64 (19)		Cu–N2–C7	121.8 (3)	
O3–Cu–N1	96.19 (18)				

Table V. Interatomic Distances (Å) and Angles (deg) Relevant to the Copper Coordination Spheres in $[Cu_4(TNL)(\mu_2\text{-}OH)_2(H_2O)_6(EtOH)_2](CF_3SO_3)_6$ (II)

Cu–O1	1.881 (5)	Cu–O3	2.406 (9)	Cu–N2	2.009 (6)
Cu–O2	1.968 (6)	Cu–N1	1.963 (7)	Cu–CuA	3.190 (2)
O1–Cu–O2	90.5 (3)		O3–Cu–N2	89.8 (3)	
O1–Cu–O3	96.3 (4)		N1–Cu–N2	90.3 (3)	
O1–Cu–N1	174.4 (4)		Cu–O1–CuA	116.0 (5)	
O1–Cu–N2	87.7 (3)		Cu–O3–CC1	131.4 (17)	
O2–Cu–O3	91.1 (3)		Cu–N1–C1	121.8 (6)	
O2–Cu–N1	91.4 (3)		Cu–N1–C5	120.7 (6)	
O2–Cu–N2	178.1 (3)		Cu–N2–N2A	116.9 (4)	
O3–Cu–N1	88.9 (3)		Cu–N2–C6	121.1 (5)	

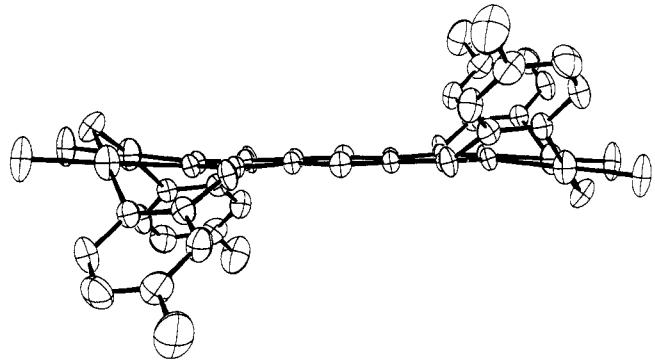

Figure 3. Structural representation of $[Cu_4(TNL4)(\mu_2\text{-}OH)_2(H_2O)_4]^{6+}$ (cation of I).

plane (0.055 (3) Å) toward O3. The copper atoms are separated by 3.202 (2) Å, and the hydroxide bridge angle is quite large (116.3 (3)°). The double-bridge arrangement in each binuclear half contrasts sharply with our previous studies on analogue pyridylamino phthalazine ligands, where, in all cases, even with hydroxide bridge angles in excess of 114°, three groups bridged the two copper centers, with an anionic bridging ligand, e.g., SO_4, NO_3, occupying the axial copper sites.[20] The benzodipyridazine moiety is flat and almost coplanar with the perfect plane defined by the atoms Cu–CuA–N2–N2A (dihedral angle 6.5 (1)°) (Figure 3), and the bridging oxygen (O1) is displaced by 0.717 (6) Å from the Cu_2N_2 mean plane. The pendant pyridine rings are twisted with respect to the benzodipyridazine group and are inclined at an angle of 41.27 (15)° with respect to the Cu_2N_2 plane. The complex cations stack along the '*a*' axis (Figure 4), with the molecular separation approximately equal to the '*a*' axis cell edge length.

The structure of II is shown in Figure 5. Interatomic distances and angles relevant to the copper coordination spheres are given in Table V. Structurally, II is very similar to I, with comparable dimensions in each binuclear half. Two ethanol molecules were found in the structure, as disordered axial ligands, with Cu–O contacts comparable with those to the axial water molecules in I. The axial ligands were modeled as half water and half ethanol and are shown as ethanol molecules in Figure 5. The copper–copper separation is slightly shorter (3.190 (2) Å), in keeping with

(20) Thompson, L. K.; Hanson, A. W.; Ramaswamy, B. S. *Inorg. Chem.* **1984**, *23*, 2459.

Table VI. Spectral and Magnetic Data

compound	ν_{OH}, cm^{-1}	λ_{max},[d] cm^{-1}	$\mu_{eff}(\mu_B)$[e]
$[Cu_4(TNL4)(\mu_2\text{-}OH)_2(H_2O)_8](CF_3SO_3)_6$ (I) green	3539	23 500 [19 000][a] 25 300 (13 600), 18 200 (320)[b] 21 300 (25 000)[c]	1.24
$[Cu_4(TNL)(\mu_2\text{-}OH)_2(H_2O)_6(EtOH)_2](CF_3SO_3)_6\cdot 3H_2O$ (II) green	3630	22 700 [19 000][a] 25 600 (13 000), [17 800] (310)[b] 21 300 (25 000)[c]	1.06
$[Cu_4(TNL)(\mu_2\text{-}OH)_2(NO_3)_4](NO_3)_2\cdot 2H_2O$ (III) brown	3528	22 700 [19 200][a]	0.96
$[Cu_4(TNL5)(\mu_2\text{-}OH)_2(H_2O)_8](CF_3SO_3)^6$ (IV) green	3498 sh	22 700 [19 000][a] 25 000 (14 700), 17 400 (300)[b] 21 500 (20 000)[c]	1.34
$[Cu_4(TNL4)(\mu_2\text{-}OH)_2Br_6(H_2O)_2]$ (V) green	3582	23 500, 16 500[a]	0.72
$[Cu_4(TNL4E)(\mu_2\text{-}Cl)_4Cl_4]\cdot 0.5MeOH\cdot 3H_2O$ (VI) green		23 000, 14 900[a]	1.80

[a] Mull transmittance. [b] CH_3CN (ϵ). [c] DMF (ϵ). [d] Brackets, ϵ for. [e] At room temperature.

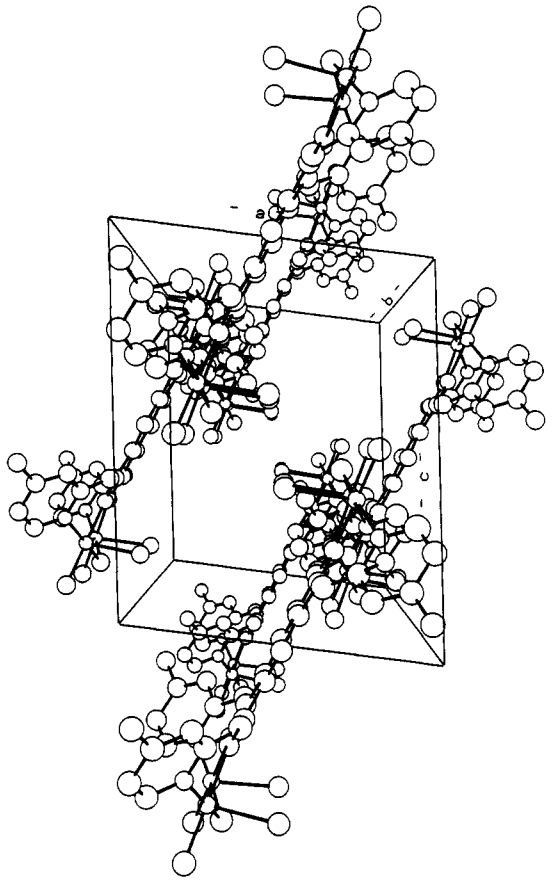

Figure 4. Packing diagram for $[Cu_4(TNL4)(\mu_2\text{-}OH)_2(H_2O)_4]^{6+}$ (cation of I).

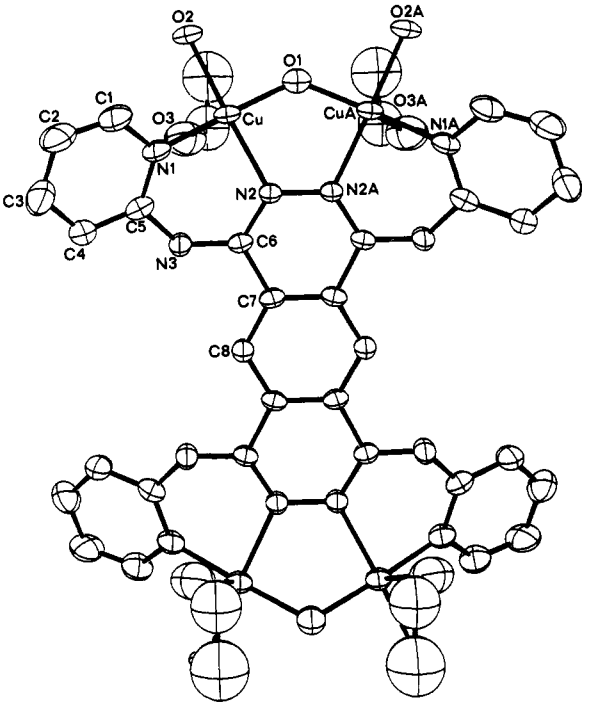

Figure 5. Structural representation of $[Cu_4(TNL)(\mu_2\text{-}OH)_2(H_2O)_6(EtOH)_2]^{6+}$ (cation of II) with hydrogen atoms omitted (40% probability thermal ellipsoids).

a comparable Cu–OH–Cu angle (116.0 (5)°). The benzodipyridazine moiety is flat and almost coplanar with the Cu_2N_2 (diazine) perfect plane (dihedral angle 10.3 (2)°), with a similar displacement of the oxygen bridge (O1) from this plane (0.686 (11) Å). A somewhat smaller twist of the pyridine rings is observed with respect to the Cu_2N_2 plane (33.2 (3)°).

Spectral and Magnetic Properties. Infrared spectra (Table VI) of all the complexes, except VI, have characteristic absorptions around 3500 cm^{-1} or above, associated with the bridging OH group, and in the case of I, II, IV, and V broad, lower energy absorptions associated with coordinated water. Far-infrared spectra for I–IV are very complex, making assignments difficult, but internal comparisons of V and VI, and with other derivatives, indicate the presence of coordinated halogen. The nitrate complex (III) exhibits two characteristic nitrate combination band absorptions at 1764 and 1722 cm^{-1}, which can be assigned to bidentate nitrate group,[21] while the other nitrates appear to be ionic, on the basis of the presence of a shoulder at ~1740 cm^{-1}.

Solid-state, mull transmittance spectra for I–IV (Table VI) are characterized by the presence of an intense charge-transfer absorption in the range 22 500–23 800 cm^{-1}, with a lower energy, less intense, shoulder around 19 000 cm^{-1}, which is assigned to a d–d transition. Freshly prepared solutions of I, II, and IV in acetonitrile again show two bands, an intense absorption around 25 000 cm^{-1} and a weak band at lower energy, clearly d–d in origin and associated with the five-coordinated copper(II) centers. Similar high-energy charge-transfer bands are observed for V and VI, and the lower energy absorptions are assigned to d–d transitions. The d–d band in VI is much lower in energy than that in V, supporting the presence of both terminal and bridging chlorine ligands in VI and a mixture of oxygen and bromine ligands in V.

Structurally complex IV is expected to be analogous to I and II, with ionic triflate and eight coordinated water molecules. Compound III is clearly a dihydroxo-bridged derivative, involving just two bridges (diazine and hydroxide) between the copper(II) centers, consistent with its very low magnetic moment. Complex V appears to have a dihydroxo-bridged five-coordinate structure, analogous to I and II, with halogens and water occupying terminal ligand positions at each copper center. Complex VI clearly does not involve hydroxide bridges and the near-normal room temperature magnetic moment suggests a double chlorine-bridged square-pyramidal structure, analogous to the complex Cu_2-

(21) Lever, A. B. P.; Mantovani, E.; Ramaswamy, B. S. *Can. J. Chem.* **1971**, *49*, 1957.

$(PAP46Me)Cl_4$ (PAP46Me = 1,4-bis((4,6-dimethylpyrid-2-yl)-amino)phthalazine).[22] In this complex an asymmetric, orthogonal, dichloro-bridged binuclear center leads to a very weakly coupled system ($-2J$ = 55 cm^{-1}).[23]

The analogous, green, five-coordinate binuclear hydroxo-bridged phthalazine complexes $[Cu_2(PAP)(OH)X_3]$ (X = Cl, Br; PAP = 1,4-bis(2'-pyridylamino)phthalazine) have d–d absorptions at 15 700 and 15 800 cm^{-1}, respectively, in the solid state and $\pi-\pi^*$ charge-transfer bands around 28 000 cm^{-1}.[10] These $\pi-\pi^*$ bands appear at 29 000 cm^{-1} in their green aqueous solutions (ϵ = 12 000 (Cl), 23 400 (Br)). For carboxylate complexes of this ligand, $[Cu_2(PAP\text{-}H)(RCOO)_3]$, involving deprotonated PAP, a substantial lowering in energy of this charge-transfer band was observed, both in the solid state (23 800–25 600 cm^{-1}) and in solution (23 200–24 800 cm^{-1}). The lower energy $\pi-\pi^*$ absorption is associated with increased π conjugation in the anionic form of the ligand. The tetranucleating ligands are all neutral in the complexes discussed, and the similarity between these ligands and PAP and its derivatives would safely indicate that the low-energy charge-transfer bands in the tetranuclear complexes are $\pi-\pi^*$ in nature. However, the average energy of this transition is lower than that observed for the anionic form of PAP in the solid state. This suggests that π conjugation occurs more readily in the neutral form of the tetranucleating ligands than in the anionic form of PAP.

Complexes, I, II, and IV are green in the solid state and freshly prepared solutions in dry acetonitrile, nitromethane, and THF are also green. Although there is a slight increase in energy of the charge-transfer band in solution in acetonitrile (25 000–25 600 cm^{-1}), which may indicate some solvent coordination, it appears that the structural integrity of the complexes has been maintained. However, in complete contrast, solutions of these complexes in DMF, DMSO, and even methanol and water are red. The red solutions of I, II, and IV in DMF show a major shift of the $\pi-\pi^*$ absorption to lower energy (~21 000 cm^{-1}; Table VI), indicating a major change in the nature of the complexes. Similar spectra were obtained in DMSO. Addition of water to the green acetonitrile solutions of I, II, and IV produced the same effect, with the formation of red solutions and the gradual shift of the charge-transfer band to lower energies. By analogy with the PAP complexes, it seems that the ligand is spontaneously undergoing proton loss in polar protic solvents, even in the absence of added base. This process was confirmed by addition of weak bases, e.g., Et_3N and aniline, to the green acetonitrile solutions, whereupon intense red solutions immediately formed, with the same spectral features. Further results and discussion on these unusual spectral changes will be presented in a future publication.

The ligands can be considered as the superposition of two (pyridylamino)phthalazine ligands (Figure 1), in which the two diazine rings are connected by a fused benzene ring, and each phthalazine-like half can accommodate two copper centers in an arrangement which resembles that in $[Cu_2(PAP)(OH)Cl_3]$[24] and other related compounds. These complexes, which involve six-membered chelate rings, have three groups bridging the two copper centers (diazine, hydroxide, and anion) in all cases except one (no anion bridge)[9] with metal–metal separations falling in the range 3.00–3.25 Å. With diazine ligands involving five-membered chelate rings, the ligand geometric constraints effectively create larger metal–metal separations, preventing the formation of a third, axial bridge, and only dibridged systems are formed (diazine and hydroxide bridges).[23] In all cases, the copper centers are antiferromagnetically coupled with propagation of spin exchange via the diazine and hydroxide bridges. In a related series of $d_{x^2-y^2}$ ground-state complexes, spin exchange has been shown to vary in a linear fashion with hydroxide bridge angle.[23] The tetranuclear complexes I and II have only two bridging groups between copper

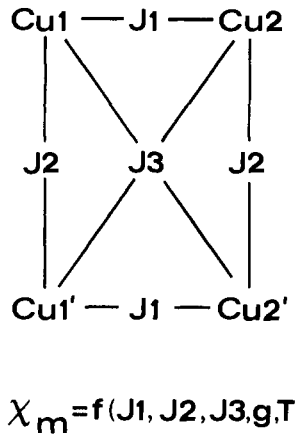

Figure 6. Rectangular magnetic exchange model (Cu1 = Cu, Cu2 = CuA; Figures 2 and 5).

centers and large copper–copper separations compared with most of the analogous binuclear complexes. This may be associated, in part, with the poor coordinating ability of the triflate anion and leads to a situation where low magnetic moments are observed, indicative of strong antiferromagnetic coupling (Table VI). The other hydroxo-bridged complexes also have low room temperature magnetic moments indicative of moderate to strong antiferromagnetic coupling.

The tetranuclear arrangement of copper(II) centers can be regarded magnetically as an isolated pair of binuclear centers, akin to the PAPR complexes, or as a rectangular arrangement with two relatively short and four long contacts (Figure 6; D_2 symmetry). In the double binuclear case, any superexchange interaction between pairs across the fused heteroaromatic framework would be considered to be negligible and significant exchange would only be considered within each binuclear unit via a superexchange mechanism involving hydroxide and diazine bridges. In this case the magnetic properties would be defined by the Bleaney–Bowers expression[25] for an interacting $S = {}^1/_2$ pair defined by the spin Hamiltonian $H = -2J\hat{S}_1\cdot\hat{S}_2$. In the rectangular case the full spin Hamiltonian (eq 1) involves three

$$H_{ex} = -2[J_1(\hat{S}_1\cdot\hat{S}_2 + \hat{S}_{1'}\cdot\hat{S}_{2'}) + J_2(\hat{S}_1\cdot\hat{S}_{1'} + \hat{S}_2\cdot\hat{S}_{2'}) + J_3(\hat{S}_1\cdot\hat{S}_{2'} + \hat{S}_2\cdot\hat{S}_{1'})] \quad (1)$$

$$\chi_m = f(J_1,J_2,J_3,g,T) + N\alpha \quad (2)$$

superexchange pathways, and three exchange integrals (J_1,J_2,J_3; Figure 6) would be required to describe the molar susceptibility (eq 2; $N\alpha$ is the temperature-independent paramagnetism). J_1 is considered to be the dominant exchange integral because of the shorter copper–copper separation, and because of the similarity of the lateral and diagonal pathways within the fused heteroaromatic framework, J_2 and J_3 can be considered to be approximately the same ($J_2 \approx J_3$). The double bridge in each binuclear half is accounted for by only one exchange term. The energy levels appropriate to eq 1[26] can be substituted into the Van Vleck equation to give the appropriate susceptibility expression and adapted for the situation where $J_2 = J_3$. The rectangular model can be corrected for trimer, dimer, and monomer impurities. Likely trimer impurities include a incompletely metalated benzodipyridazine species or a trinuclear complex of a mixed phthalazine–isoindoline ligand, resulting from incomplete reaction with hydrazine during ligand synthesis. Such a species would behave effectively as a "monomeric" impurity. Reasonable dimeric impurities would correspond to two possible derivatives, one with two coppers bound in juxtaposition on one phthalazine half and the other with one copper on each side of the benzodipyridazine

(22) Mandal, S. K.; Thompson, L. K.; Newlands, M. J.; Lee, F. L.; LePage, Y.; Charland, J.-P.; Gabe, E. J. *Inorg. Chim. Acta* **1986**, *122*, 199.
(23) Thompson, L. K.; Lee, F. L.; Gabe, E. J. *Inorg. Chem.* **1988**, *27*, 39.
(24) Marongiu, G.; Lingafelter, E. C. *Acta Crystallogr., Sect. B: Struct. Crystallogr. Cryst. Chem.* **1982**, *B38*, 620.
(25) Bleaney, B.; Bowers, K. D. *Proc. R. Soc. London* **1952**, *A214*, 451.
(26) Jotham, R. W.; Kettle, S. F. A. *Inorg. Chim. Acta* **1970**, *4*, 145.
(27) Thompson, L. K.; Mandal, S. K.; Charland, J.-P.; Gabe, E. J. *Can. J. Chem.* **1988**, *66*, 348.

Table VII. Magnetic Data

compound	$g_{(av)}$	J_1, cm^{-1}	J_2, cm^{-1}	X^a	Y^b	10^2R^c
$[Cu_4(TNL4)(\mu_2\text{-}OH)_2(H_2O)_8](CF_3SO_3)_6$ (I)	2.04 (2)	−167 (3)	−60 (5)	0.034	0.066	2.7
$[Cu_4(TNL)(\mu_2\text{-}OH)_2(H_2O)_6(EtOH)_2](CF_3SO_3)_6$ (II)	2.01 (3)	−218 (4)	−36 (5)	0.026	0.026	2.5
$[Cu_4(TNL)(\mu_2\text{-}OH)_2(NO_3)_4](NO_3)_2\cdot 2H_2O$ (III)	2.04 (3)	−251 (6)	−160 (10)		0.048	1.1
$[Cu_4(TNL4)(\mu_2\text{-}OH)_2Br_6(H_2O)_2]$ (V)	2.06 (2)	−338 (2)	−210 (10)	0.02	0.029	1.72
$[Cu_4(TNL4E)(\mu_2\text{-}Cl)_4Cl_4]\cdot 0.5MeOH\cdot 3H_2O$ (VI)	2.046 (1)	−7.96 (2)	11.8 (2)			0.28

[a] X, dimer fraction. [b] Y, monomer fraction. [c] $R = \{\sum(\chi_{obs} - \chi_{calc})^2/\sum(\chi_{obs})^2\}^{1/2}$; TIP = 60×10^{-6} cgsu (TIP = 70×10^{-6} for III).

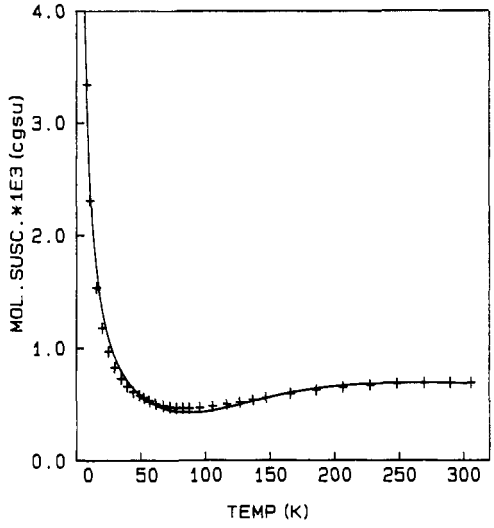

Figure 7. Magnetic susceptibility data for $[Cu_4(TNL)(\mu_2\text{-}OH)_2(H_2O)_8](CF_3SO_3)_6$ (I). The solid line was calculated from eq 3 with g = 2.04 (2), J_1 = −167 (3) cm^{-1}, $J_2 = J_3$ = −60 (5) cm^{-1}, X = 0.034, Y = 0.066.

ring system. Of the two, the former seems the most likely based on the high stability of hydroxo-bridged phthalazine derivatives. Equation 3 includes both monomer (fraction Y) and dimer (fraction X) corrections and assumes that $J_2 = J_3$.

$$\chi_m(\text{total}) = f(J_1,J_2,g,T)(1 - X - Y) + Xf(J_1,g,T) + Yf(g,T) + N\alpha \quad (3)$$

Variable-temperature magnetic susceptibility measurements were carried out on powdered samples of I–III and V in the temperature range 5–305 K. Figure 7 illustrates a typical plot of χ_m vs temperature for the dihydroxo-bridged derivative I, with a rise in χ_m at high temperature indicative of strong antiferromagnetic exchange and a rapid rise in χ_m at low temperature indicative of the presence of significant paramagnetic impurity. Attempts to fit the data for the hydroxo-bridged compounds I–III and V to the Bleaney–Bowers expression for an essentially isolated pair of binuclear centers were not successful unless large, negative Weiss corrections were employed. This indicates that significant interdimer coupling is present. The variable-temperature magnetic data were fitted to a variety of models based on the rectangular tetramer, with corrections for trimeric, dimeric, and monomeric impurities in a variety of combinations. The values of J_1 and J_2 fell into fairly narrow ranges (e.g., J_1 −155 to −170 cm^{-1}; J_2 −50 to −95 cm^{-1} for I with sensible g values) for all the models chosen, but a model based on eq 3 in general gave the lowest R values (Table VII). However, the data fits for I and II were not very sensitive to small changes in the derived parameters during the iterative process, and the minimization of the residual function followed a rather shallow curve, reflecting the difficulty of including five parameters in the regression analysis. The best-fit analyses (eq 3) of the data for I and II are given in Table VII, and the experimental data and the theoretical line fit for I for $g_{(av)}$ = 2.04 (2), J_1 = −167 (3) cm^{-1}, J_2 = −60 (5) cm^{-1}, X = 0.034, and Y = 0.066 are shown in Figure 7. The major spin-exchange interaction (J_1) for compounds I and II is antiferromagnetic, takes place between the adjacent copper centers in each dimer half, and results from superexchange via the hydroxide and diazine bridges. The presence of very large hydroxide bridge angles for I and II indicates that the hydroxide bridge would be expected to dominate the exchange process.[23] However, the remarkable result is that significant cross-ring antiferromagnetic coupling also occurs for these compounds across eight or nine bond connections, depending on the route (e.g., 12.34 or 13.72 Å for I).

The hydroxide bridge angles for I and II are comparable with the upper limit of this angle in a series of related, tribridged binuclear copper phthalazine complexes.[23] Exchange integrals (-2J) around 540 cm^{-1} would be expected for a bridge angle of ~116°, based on the linear relationship between -2J and the Cu–OH–Cu angle observed in this series. The reduced direct exchange indicated by the J_1 values for I and II suggests a different charge distribution in the tetranuclear complexes. By comparison of related binuclear copper phthalazine and pyridazine complexes it has been shown that charge delocalization from the copper atoms extends into the fused benzene ring in the phthalazine bridge. This has the effect of reducing antiferromagnetic coupling between the copper(II) centers in the phthalazine complexes in comparison with the pyridazine derivatives.[23,28] The significant cross-ring coupling in I and II clearly indicates that copper charge has been delocalized into the fused benzene ring, some of which is coupled antiferromagnetically, but some may be capacitively stored in the aromatic system, as is the case in the phthalazine derivatives. The larger J_2 value for II, compared with I, may be a reflection on the larger dihedral angle between the Cu_2N_2 (diazine) planes and the benzodipyridazine plane (6.5° (I), 10.3° (II)). This would imply weaker cross-ring exchange, resulting from less efficient overlap of the copper magnetic orbitals with the planar benzodipyridazine ring system, and also allow greater exchange between the copper atoms in each dimer half, as indicated by the more negative J_1 value for II.

Complexes III and V have susceptibility/temperature profiles similar to that of I and very low room temperature magnetic moments indicative of strong net antiferromagnetic coupling. Fitting of the data for III and V to the Bleaney–Bowers equation required large, negative Weiss corrections (<−150 K) but gave -2J values (389 (2) cm^{-1} (III), 585 (4) cm^{-1} (V)) consistent with strong intradimer antiferromagnetic exchange. Fitting of the data for V to eq 3 with the J_2 iteration range set between −270 and −50 cm^{-1} gave reasonable g values and large negative values for J_1 and J_2 (Table VII). J_2 values were found in the range −190 to −210 cm^{-1} for several regression analyses involving different iteration limits. However changes in R values were small, but significant. The large, negative J_1 value is consistent with the Bleaney–Bowers fit and indicates very strong intradimer coupling. However, in the absence of structural details on this compound, the most obvious suggestion for enhanced cross-ring coupling would be the near-perfect alignment of the copper magnetic orbitals with appropriate orbitals in the planar benzodipyridazine ring system. The nitrate complex III has a slightly larger room temperature magnetic moment, indicative of somewhat weaker net antiferromagnetic exchange. Fitting of the variable-temperature magnetic data to eq 3 proved to be more difficult for this compound, and the equation was simplified by only including a paramagnetic impurity correction. A reasonable regression was obtained with a slightly adjusted TIP (70×10^{-6} cgsu). The J_1 value is consistent with the Bleaney–Bowers fit and indicates strong intradimer antiferromagnetic exchange. Strong cross-ring antiferromagnetic coupling is also observed for this compound, indicating efficient

(28) Mandal, S. K.; Thompson, L. K.; Newlands, M. J.; Gabe, E. J.; Nag, K. *Inorg. Chem.* **1990**, *29*, 1324.

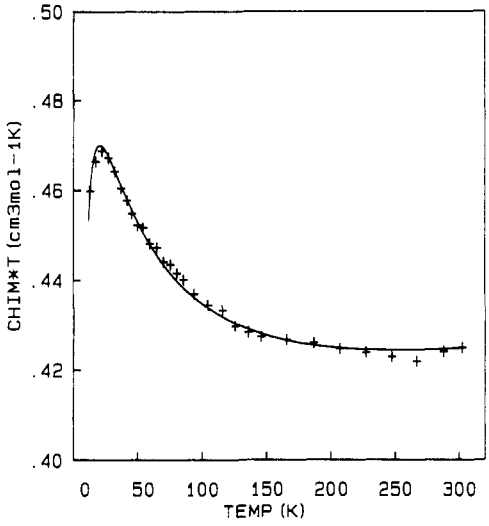

Figure 8. Magnetic susceptibility data for $[Cu_4(TNL4E)(\mu_2\text{-}Cl)_4Cl_4]$ (VI). The solid line was calculated from eq 3 with $g = 2.046$ (1), $J_1 = -7.96$ (2) cm^{-1}, $J_2 = 11.8$ (2) cm^{-1} ($X = 0$, $Y = 0$).

spin communication between the copper centers across the benzodipyridazine rings.

Compound VI presents an interesting contrast to the hydroxo-bridged complexes. Analytical data confirm the presence of eight chlorine atoms, and spectral data indicate the absence of a hydroxide bridge. The variable-temperature (10–305 K) magnetic data for VI (Figure 8), plotted as $\chi_m T$ vs T, indicate very different behavior from the other complexes and the presence of a dominant, weak, ferromagnetic interaction. The sharp drop in $\chi_m T$ below ~25 K is indicative of the presence of antiferromagnetic coupling as well. The magnetic moment rises from a value of $\mu_{eff} = 1.80\mu_B$ at room temperature to $1.93\mu_B$ at 22.3 K, dropping at lower temperatures. The experimental susceptibility data were fitted to the rectangular model (eq 3), giving $g = 2.046$ (1), $J_1 = -7.96$ (2) cm^{-1}, $J_2 = 11.8$ (2) cm^{-1} ($X = 0$, $Y = 0$). The best-fit line is shown in Figure 7. Since the fit of these data is so good, far more confidence can be placed in the assignment of J_1 and J_2 than for the other complexes. The antiferromagnetic intradimer exchange in VI is consistent with the situation observed for the related complex $[Cu_2(PAP46Me)Cl_4]$ ($-2J = 55.2$ cm^{-1}),[23] which involves two orthogonally bridging chlorines in a distorted square-pyramidal structure. In this complex the weak antiferromagnetic coupling is presumed to occur via the phthalazine bridge only. The reduced antiferromagnetic exchange (J_1) in VI could be associated with a structural difference in the binuclear unit, leading to less efficient copper magnetic orbital overlap with the diazine bridge or, perhaps, an inductive effect associated with different pyridine ring substituents. However, the dominant, cross-ring, ferromagnetic coupling is surprising but may be the result of a much larger dihedral angle between the Cu_2N_2 planes and the benzodipyridazine plane. The weakened antiferromagnetic cross-ring coupling associated with an increased dihedral angle between the Cu_2N_2 plane and the benzodipyridazine plane (I, II) could lead to a crossover of cross-ring coupling from antiferromagnetic to ferromagnetic with more severe distortion. We must, however, await structural details on more of these complexes to substantiate this situation.

The significant antiferromagnetic, cross-ring, coupling observed for I and II, and the much stronger coupling for III and V propagated over such large distances, is most unusual and can be attributed to the essentially flat nature of the rectangular array of copper centers relative to the heterocyclic bridge, and good overlap of the corresponding orbitals with the magnetic copper $d_{x^2-y^2}$ orbitals. The low-energy π–π^* absorptions observed for these systems and the presence of a highly conjugated, fused aromatic network suggest that the cross-ring coupling between copper pairs occurs, at least in part, by a π mechanism. The apparent cross-ring ferromagnetic coupling in VI is quite unexpected and suggests a more distorted structural arrangement of the copper center relative to the heterocyclic ring system. We are examining more complexes of this sort from the standpoint of their magnetostructural and magnetoelectronic properties.

Acknowledgment. We thank the natural Sciences and Engineering Research Council of Canada for financial support for this study and Punjabi University, Patiala, India, for granting leave of absence to S.S.T.

Supplementary Material Available: Tables listing thermal parameters (SI and SII), distances and angles (SIII and SIV), and least-squares planes data (SV and SVI), for I and II, respectively, and calculated hydrogen positional parameters for II (SVII) and figures showing packing stereoviews of I and II (20 pages); tables of observed and calculated structure factors for I and II (31 pages). Ordering information is given on any current masthead page.